HHS Public Access

In situ programming of leukaemia-specific T cells using synthetic DNA nanocarriers

Tyrel T. Smith[1,†], **Sirkka B. Stephan**[1,†], **Howell F. Moffett**[1,†], **Laura E. McKnight**[1], **Weihang Ji**[1], **Diana Reiman**[2], **Emmy Bonagofski**[2], **Martin E. Wohlfahrt**[1], **Smitha P. S. Pillai**[3], and **Matthias T. Stephan**[1,2,4,5,*]

[1]Clinical Research Division, Fred Hutchinson Cancer Research Center, Seattle, Washington 98109, USA

[2]Technology Access Foundation (TAF) Academy, Fred Hutchinson Cancer Research Center, Seattle, Washington 98109, USA

[3]Comparative Pathology, Fred Hutchinson Cancer Research Center, Seattle, Washington 98109, USA

[4]Department of Bioengineering and Molecular Engineering & Sciences Institute, University of Washington, Seattle, Washington 98105, USA

[5]Department of Medicine, Division of Medical Oncology, University of Washington, Seattle, Washington 98109, USA

Abstract

An emerging approach for treating cancer involves programming patient-derived T cells with genes encoding disease-specific chimeric antigen receptors (CARs), so that they can combat tumour cells once they are reinfused. Although trials of this therapy have produced impressive results, the *in vitro* methods they require to generate large numbers of tumour-specific T cells are too elaborate for widespread application to treat cancer patients. Here, we describe a method to quickly program circulating T cells with tumour-recognizing capabilities, thus avoiding these complications. Specifically, we demonstrate that DNA-carrying nanoparticles can efficiently introduce leukaemia-targeting CAR genes into T-cell nuclei, thereby bringing about long-term disease remission. These polymer nanoparticles are easy to manufacture in a stable form, which simplifies storage and reduces cost. Our technology may therefore provide a practical, broadly

applicable treatment that can generate anti-tumour immunity 'on demand' for oncologists in a variety of settings.

Despite the obvious advantages afforded by targeted T-cell therapies (compared with the blunt instruments of chemotherapy, radiation and surgery), the complex procedures and costs involved in producing genetically modified lymphocytes remain major obstacles for implementing them as standard-of-care in the treatment of cancer[1,2]. Currently, clinical-scale manufacturing of T lymphocytes requires an assortment of elaborate protocols to isolate, genetically modify, and selectively expand the redirected cells before infusing them back into the patient. Because these difficult procedures entail dedicated equipment and considerable technical expertise, they can only be performed at a few specialized centres worldwide. Given the challenges this disease already poses to our healthcare system, providing personalized T-cell therapy to the more than 1.5 million new patients diagnosed just in the United States each year is not practical.

Nanotechnology could solve this problem by making available inexpensive DNA carriers that can quickly and specifically program tumour-recognizing capabilities into T cells as they circulate within the patient (Supplementary Fig. 1). Here, we demonstrate that once they are adapted with lymphocyte-targeting ligands, polymeric nanocarriers can selectively deliver leukaemia-specific CAR genes into host T cells *in situ.* When administered under the correct conditions, these particles can program T cells in quantities that are sufficient to bring about tumour regression with efficacies that are similar to conventional infusions of T cells transduced *ex vivo* with CAR-encoding viral vectors. We found that nanoparticle-reprogrammed T cells continue to produce these receptors for weeks, allowing them to act as a 'living drug' that increases in number, serially destroys tumour cells, and ultimately differentiate into long-lived memory T cells.

Designing nanocarriers to achieve CAR expression in T cells

To achieve effective nucleic acid delivery into T cells, gene carriers must (i) be taken up by T cells and (ii) import their DNA cargo into the cell nucleus. Our first step was to couple T-cell-targeting anti-CD3e f(ab′)2 fragments to the surfaces of biodegradable poly (β-amino ester)-based nanoparticles[3], which selectively enabled their receptor-mediated endocytosis by lymphocytes (Fig. 1a). To achieve requirement (ii), we functionalized the polymer with peptides containing microtubule-associated sequences (MTAS) and nuclear localization signals (NLS), as a means to facilitate fast-track nuclear import of their genetic cargo via the microtubule transport machinery[4].

We furnished these targeted nanoparticles with anticancer programming capabilities by loading them with plasmid DNA encoding the leukaemia-specific 194-1BBz CAR (ref. [5]), which is a fusion receptor composed of a single-chain antibody (scFv) specific for the extracellular domain of the CD19 leukaemia antigen, combined with 4-1BB and CD3ζ cytoplasmic signalling domains. To conduct our studies in immunocompetent mice, we used an all-murine CAR that is equivalent to one that is the focus of current clinical trials[6]. We achieved persistent CAR expression in actively dividing T cells by flanking our gene expression cassette with piggyBac inverted terminal repeats; these transposons are mobile

genetic elements that efficiently integrate vectors into chromosomes via a cut-and-paste mechanism[7], an event that is mediated by the piggyBac transposase enzyme. To enable this integration, we co-encapsulated a plasmid encoding a hyperactive form of the transposase (iPB7)[8] into the carriers.

The nanoparticles were manufactured by mixing the reactants at a polymer:DNA ratio of 30 (w/w) in aqueous conditions, which condenses plasmid DNA into nanosized complexes (Fig. 1 and Supplementary Fig. 2). These were targeted towards T cells by coupling polyglutamic acid to anti-CD3e f(ab′)2, forming a conjugate that was electrostatically adsorbed to the particles. The resulting DNA nanocarriers were 155 ± 40 nm in size and -7.8 ± 2.1 mV in zeta potential, and could be lyophilized prior to use with no change in properties or efficacy (Fig. 1 and Supplementary Fig. 2).

CAR-programming of cultured T cells via DNA nanocarriers

We first assessed the ability of the engineered nanoparticles to program specificities against leukaemia by incubating mouse splenocytes with the particles at various ratios. We found that CD3-targeted nanoparticles selectively bind T lymphocytes, as their interactions with off-target cells were low (Fig. 2a). Confocal imaging established that the particles are rapidly (120 min) internalized into the cytoplasm, presumably as a result of receptor-induced endocytosis (Fig. 2b). As early as 30 h post-transfection, 194-1BBz receptors were detected on the surfaces of the treated cells (mean 3.8% CAR$^+$ T cells $\pm$ 0.3%, nanoparticle:T cell ratio = 3×10^3:1; Fig. 2c). Gene transfer greatly benefited from the use of poly(beta-amino ester) (PBAE) polymer that had been functionalized with the MTAS and NLS sequences, as in their absence nuclear targeting of CAR-transgene expression in primary T cells was substantially lower (mean $1.1 \pm 0.2\%$; Fig. 2d). Nanoparticle-transfected lymphocytes were fully functional, as they selectively lysed Eµ-ALL01 leukaemia cells and secreted effector cytokines at levels similar to T cells transduced with a lentiviral vector encoding the same CAR (Fig. 2e–g). Exposure of T cells to anti-CD3e f(ab′)2 on the surfaces of the nanoparticles resulted in only a mild T-cell stimulation compared with untargeted particles, and did not induce unresponsiveness to antigen restimulation (Supplementary Fig. 3). Incorporating piggyBac transposable elements into nanoparticle-delivered plasmids maintained high-level 194-1BBz gene expression in T cells over many days as a result of somatic integration (Fig. 2h and Supplementary Fig. 4).

In vivo T-cell targeting and reprogramming

Our goal is to selectively edit lymphocyte targeting *in vivo* to bring about the regression of cancer; accordingly, we next examined how exclusively CD3-mediated targeting confined nanoparticle interactions to circulating T cells by systemically injecting mice with 3×10^{11} functionalized, DNA-free nanoparticles that we fluorescently tagged. Flow cytometry of peripheral blood collected 4 h later established that 34% ($\pm$5.1%) of the circulating T lymphocytes bound CD3-targeted nanoparticles, whilst signals from offtarget cells in peripheral blood were low ($5.9 \pm 2.8\%$; Fig. 3a). A more detailed phenotypic analysis revealed that neutrophils, monocytes and B cells were among the more prominent subtypes that non-specifically bound injected CD3-targeted nanoparticles, although particles were

also detected on small numbers of natural killer (NK) cells and eosinophils (Fig. 3a, lower panel, that is, the horizontal bar in the middle showing the different cell populations). As *in vitro*, confocal microscopy of sorted T cells confirmed the rapid internalization of bound nanoparticles from the cell surface (Fig. 3a, right panel). As *in vitro* means that the confocal picture shown in the right panel of Fig. 3a show the same process (receptor-mediated internalization of nanoparticles by T cells) as Fig. 2b (*in vitro* experiments). The difference in Fig. 3 compared to Fig. 2 is that in Fig. 3 nanoparticles were injected intravenously into mice and taken up *in vivo* whereas in Fig. 2 nanoparticles were directly incubated with T cells *in vitro.* The right panel refers to the confocal image of T cells with incorporated nanoparticles. Infused nanoparticles were taken up by all CD3-expressing T-cell subpopulations, including CD4^{+} and CD8^{+} naive, effector and memory cells, in numbers reflecting their respective physiological ratios in peripheral blood (Fig. 3b). In parallel experiments, we quantified the distribution of nanoparticles in various organs 4 h after intravenous injection. The highest concentrations of non-targeted particles were found in the liver, whilst lymphocyte-targeted nanocarriers accumulated mainly in the spleen, lymph nodes and bone marrow (Fig. 3c,d).

Guided by the distribution data, we next measured potential *in vivo* toxicities of the lymphocyte-targeted nanocarriers. These experiments were conducted using nanoparticles loaded with P4-1BBz genes (which encode a CAR specific for human prostate-specific membrane antigen[9]) instead of those encoding the 194-1BBz CAR, thereby ensuring that any changes in the parameters we measured (for example, blood levels of cytokines) could be attributed to the nanocarriers per se rather than their reprogramming activity. Mice were injected with five daily doses of 3×10^{11} nanoparticles, or phosphate-buffered saline as a control. Gross examinations and histopathology performed 24 h after the final dose revealed no treatment-related macro- or microscopic lesions (Supplementary Fig. 5a–c). Cell counts and blood chemistry profiles also revealed no abnormalities, indicating that systemic toxicities did not occur (Supplementary Fig. 5d). In addition, nanoparticle treatments caused only modest increases in the expression levels of inflammatory cytokines (interferon gamma: 1.6-fold, $P = 0.51$, non-significant (ns) ($P>0.05$); interleukin-12: 1.3-fold, $P = 0.015$* (* means significant); interleukin-6: 2.5-fold, $P = 0.01$*; Supplementary Fig. 5d).

To determine if the targeted nanoparticles can reprogram circulating T cells with leukaemia-specific CAR genes *in situ*, we intravenously injected mice bearing B-cell acute lymphoblastic leukaemia with five sequential doses of 3×10^{11} nanoparticles engineered to deliver transgenes encoding the 194-1BBz CAR. One treatment group received nanoparticles carrying the CAR transgene only, and a second group was injected with particles co-delivering the CAR transgene with plasmids encoding iPB7 transposase, which mediates efficient integration of nanoparticle-delivered CAR transposons into the genome of transfected T cells. A third group of mice received nanoparticles loaded with tumour-irrelevant P4-1BBz genes, and controls received no treatment. We found that only bolus injections of nanoparticles co-delivering 194-1BBz and iPB7 transgenes rapidly and efficiently programmed peripheral T cells to recognize leukaemia cells (mean 5.8% CAR^{+} among CD3^{+} $\pm$ 0.9% on day 6; Fig. 4a). Following transfection, these lymphocytes underwent robust proliferation (5.5-fold, day 12) while maintaining high-level expression of the CAR transgene (mean 7.1% CAR^{+} among CD3^{+} $\pm$ 1.7% on day 24). Following a

contraction period, nanoparticle-programmed effector T cells acquired a CD44^{high} CD62L$^+$ memory phenotype (Fig. 4a). Expansion of 194-1BBz-programmed T cells was dependent on their interaction with tumour antigens, as lymphocytes programmed with P4-1BBz CARs failed to proliferate and gradually declined to undetectable levels by day 12. Also, stable integration of the 194-1BBz transposon into the genome of transfected T cells was required to yield relevant numbers of CAR T cells, as T cells transfected with CAR-encoding nanoparticles carrying transgenes without the piggyBac elements failed to expand, even in the presence of abundant tumour antigen (Fig. 4a).

To measure the dynamics of nanoparticle-mediated programming of circulating T cells, we injected mice with particles carrying plasmids that co-express the click beetle red luciferase (CBR-luc) reporter along with CAR genes. Using bioluminescence imaging, we found that the initial signal in mice receiving treatments encoding 194-1BBz (+iPB7) was concentrated in the spleen area as early as 3 days after nanoparticle administration (Fig. 4b). This signal subsequently became systemic, spreading to areas of the bone marrow and lymph nodes while increasing in intensity (to a maximum of 41-fold on day 12; Fig. 4c). By contrast, we could detect only a weak bioluminescence signal at day 3 in mice injected either with 194-1BBz- (no iPB7 transposase) or P4-1BBz-programming nanoparticles, which gradually declined to near-background levels by day 12.

We engineered the nanoparticles to minimize off-target binding by anchoring T-cell-specific targeting ligands to their surfaces, and by shielding the nucleic acids they carry with a negatively charged polyglutamic acid coating. Nonetheless, a fraction of injected nanocarriers was cleared from the circulation by phagocytic cells of the reticuloendothelial system (for example, $16.2 \pm 3.2\%$ just by liver-resident phagocytes; Fig. 3c,d). To determine whether phagocytes that internalize DNA nanocarriers express the transgenes they take up, we quantified off-target CAR expression over time in the liver and the spleen. We found that one day after the last of the five nanoparticle doses (day 6), less than 1% of phagocytes in the liver and in the spleen expressed the nanoparticle-delivered genes (Supplementary Fig. 6). Importantly, while the percentage of CAR-transfected cells among circulating T cells increased from 5.8% ($\pm 0.9\%$) to 19.7% ($\pm 4.1\%$) between day 6 and day 12 (Fig. 4a), the fraction of nanoparticle-transfected phagocytes in the liver and the spleen gradually decreased during the same time, indicating that CAR expression in these cell types does not trigger expansion or proliferative signals.

Nanoparticle-induced anti-tumour activities

To determine whether nanoparticle-redirected T cells are produced in quantities sufficient to reduce established cancers, we systemically injected luciferase-expressing Eμ-ALL01 leukaemia cells (an immunocompetent mouse model of B-cell acute lymphoblastic leukaemia that recapitulates the disease at genetic, cellular and pathologic levels[6]) into albino C57BL/6 mice and used bioluminescent imaging to quantify differences in tumour progression between treatment groups. We found that injections of lymphocyte-targeted nanoparticles carrying P4-1BBz genes provided no improvements over controls, as mice comprising both groups had the same longevity (median survival: 13 versus 14 days, respectively; $P = 0.51$; Fig. 5a–c). By contrast, when we injected nanocarriers that

programmed 194-1BBz (+iPB7 transposase), tumours were eradicated in seven out of ten mice, and the others showed substantial regression along with an average 58-day improvement in survival; Fig. 5a–c). As CD19 is expressed on B cells—both healthy and malignant alike—we found dramatically reduced B-cell numbers in the spleens of 194-1BBz(+iPB7)-nanoparticle-treated animals (7.4×10^4 B cells/spleen $\pm 8.3 \times 10^4$ on day 12; Fig. 5d), which is consistent with the reversible B-cell aplasia observed in patients following CD19 CAR-T-cell therapy[10]. In agreement with the inefficient programming of 194-1BBz CAR T-cells using nanoparticles that carry 194-1BBz genes only (Fig. 4a–c), we saw only an average 5-day survival benefit in this treatment group compared with untreated control animals (Fig. 5c).

To compare the therapeutic efficacy of nanoparticle infusions with conventional adoptive T-cell therapy, we treated an additional group of mice with a single dose of 5 million cells transduced *ex vivo* with lentiviral vectors encoding the 194-1BBz CAR. This quantity is equivalent to the higher doses of CAR T-cells used in current clinical studies, where patients have been treated with up to 1.2×10^7 CAR T-cells per kilogram of body weight[11]. To model clinical protocols of ongoing adoptive T-cell therapy trials, which usually require preconditioning chemotherapy of patients prior to CAR-transduced cell infusion[12], CAR T-cell-treated mice received 100 mg kg^{-1} cyclophosphamide intraperitoneally a day before T-cell transfer to eliminate endogenous lymphocytes. We found that survival is greatly improved in mice treated with these transduced T cells, but not significantly better than those treated with synthetic nanoparticles programming the same receptors into circulating lymphocytes (Fig. 5a–c).

In summary, nanoparticles carrying genes of CD19-specific CARs can selectively and quickly edit T-cell specificity *in vivo* to bring about leukaemia regression in mice at efficacies comparable to conventional adoptive transfer of laboratory-manufactured CAR T-cells.

Conclusions

The results described here establish for the first time that synthetic nanoparticles can be engineered to program antigen-recognizing capabilities into lymphocytes *in vivo*.

Our approach patently contrasts with those currently used to generate T cells with defined specificities against tumours, which require isolation of T cells from the patient's blood and their genetic modification via complex laboratory procedures based on retroviral or lentiviral vectors[1,13,14].

We performed our experiments using a syngeneic, immune-competent model of B-cell acute lymphoblastic leukaemia that not only measures direct anticancer activities of nanoparticle-programmed CAR T-cells, but also recapitulates other interactions that may affect their eradication of tumours (for example, cell trafficking or immune suppressor cells)[6]. This model also enabled us to evaluate toxicities of nanoparticle treatments (Supplementary Fig. 5). By contrast, preclinical adoptive T-cell therapy studies have mostly relied on xenogeneic

models involving immunodeficient animals that do not accurately reflect tumour microenvironments and interactions between T cells and tissues[15–17].

Our test system involved treating leukaemia using 194-1BBz CAR-encoding transgenes. We chose this receptor because it is currently by far the most investigated CAR (there are 36 ongoing clinical trials internationally), and most lead-product candidates developed by cellular immunotherapy companies target CD19 (ref. [18]). Certainly, treating solid tumours using this nanotechnology platform will be more challenging: unlike leukaemia cells, which universally express high levels of CD19 target antigen and are easily accessible by circulating T cells, solid cancers are heterogeneous and protected[19]. One approach we are developing to address these problems is to program T cells with multiple CARs recognizing several cancer antigens. Another is to perform genome editing to prevent the action of tumour-stimulated checkpoint inhibitors.

Clinical implementation of nanoparticle-mediated T-cell programming will heavily rely on the safety of the procedure. We chose poly(β-amino ester) polymer, which has a half-life between 1 and 7 h in aqueous conditions[3], as the core material for T-cell-targeted nanocarriers, and shielded their positive charge to reduce off-target binding. PBAE-based nanoparticles have previously been described as safe and effective DNA delivery vectors[3,20,21], albeit using local (and untargeted) rather than systemic application. The question of whether the potential benefits of *in situ* T-cell programming outweigh safety concerns regarding gene transfer into off-target cells must still be evaluated, either in a nonhuman primate model or directly in a phase-1 dose-escalation trial. In our project, we found that even though a fraction of T-cell-targeted DNA nanocarriers is taken up by phagocytes, the transgenes they carry are not (or are only inefficiently) expressed, and the cells do not remain stably transduced (Supplementary Fig. 6). It is well known that gene transfer into phagocytes is notoriously difficult, as they are bestowed with degradative enzymes that destroy nucleic acid integrity[22]. Furthermore, the limited proliferative nature of phagocytes does not favour nuclear entry and integration of the delivered transgenes. This sharply contrasts with lymphocytes, which undergo substantial clonal proliferation and differentiation into effector cells following antigen encounters. This, and the fact that the signalling domains of CARs are specifically designed to mimic T-cell-intrinsic stimulatory signals, leads us to conclude that toxicities arising from CAR expression in non-T cells would at most be minimal, and manageable in a clinical setting. To completely eliminate this risk, the nanoparticle-delivered CAR transgenes could be expressed under the control of a T-cell-specific promoter[23,24]. Compared with the ubiquitous EF-1 alpha promoter we chose for our studies, cell-specific promoters have a weaker transcriptional activity—but thanks to the emergence of adoptive T-cell therapy, improved vector systems that enable tighter control of gene expression in T cells are in development[25].

The clinical safety of this approach would further benefit from using a transposon/transposase system that is already used in clinical trials to introduce CAR transgenes into patient T cells *ex vivo*. In particular, the Sleeping Beauty transposon has demonstrated efficient transposition and safety in several phase-1 clinical CAR T-cell trials[26]. Compared with conventional lentiviral vectors, which preferentially integrate into highly expressed cancer-related genes, this transposase mediates transgene integration into safe harbour loci

that are not expected to cause mutagenesis[27]. To exclude the possibility of unintentionally integrating antibiotic resistance genes into the host genome, early clinical testing of nanoparticle-mediated CAR T-cell programming will also likely require that nanoparticle-delivered genetic materials be in the form of minicircles[28]. Compared with the conventional plasmids we used in our current studies, minicircles are smaller, supercoiled DNA molecules; they also lack a bacterial origin of replication and an antibiotic resistance gene[29].

In summary, our findings establish that circulating T cells can be modified to express leukaemia-specific CARs using genes carried by polymeric nanoparticles, thereby enabling them to mediate rejection of the disease. Nanoparticles are easy to manufacture and are stable, which simplifies long-term storage and reduces cost. Thus, implemented in the clinic as a new form of active immunotherapy, this technology could provide a practical, low-cost, broadly applicable way to treat cancer.

Methods

Methods and any associated references are available in the online version of the paper.

Methods

Plasmid construction

All of the plasmids used in this project were custom-cloned by vectorbuilder.com.

The following piggyBac transposon gene expression vectors were used:

1.   pPB-EF1alpha-murine194-1BBz-P2A-GFP-WPRE-BGH polyA

     In this construct, a previously described all-murine CD19-specific CAR[6] is expressed under the control of the EF1alpha promoter. The only difference between this and the original 1928z CAR (which is composed of a rat anti-mouse CD19 scFv fused to the mouse CD8 transmembrane region, mouse CD28 signal transduction domain, and mouse CD3 cytoplasmic domains), is the use of the mouse 4-1BB instead of the CD28 costimulatory domain. To assess gene-transfer efficiency and monitor *in situ* T-cell programming, we created a bicistronic genetic construct that co-expresses green fluorescent protein (GFP) along with the m194-1BBz CAR by using a P2A peptide sequence. To increase gene expression, we placed a woodchuck hepatitis virus posttranscriptional regulatory element (WPRE) between the stop codon and the bovine growth hormone (BGH) poly-A signal.

2.   pPB-EF1alpha-murine194-1BBz-P2A-CBR-WPRE-BGH polyA

     Instead of GFP, this version co-expresses the 194-1BBz CAR with click beetle red luciferase (CBR)[30], to visualize nanoparticle-programmed CAR^{+} T cells *in situ* using bioluminescence imaging.

3.   pPB-EF1alpha-P4-1BBz-P2A-GFP-WPRE-BGH polyA

4.   pPB-EF1alpha-P4-1BBz-P2A-CBR-WPRE-BGHpolyA

These two control plasmids contain the same component as plasmids (1) and (2), respectively, but encode the tumour-irrelevant P4-1BBz CAR (ref. [9]) instead of the leukaemia-specific 19-41BBz CAR. P4-1BBz retargets T lymphocytes to prostate-specific membrane antigen (PSMA), a protein expressed in prostate cancer cells and the neovasculature of various solid tumours in humans, but absent in mice.

The following regular plasmid gene expression vector was used:

pRP-EF1alpha-iPB7transposase-WPRE-SV40 polyA

This plasmid encodes the hyperactive iPB7 piggyBac transposase[8] under the control of the EF1alpha promoter. A WPRE sequence was inserted between the stop codon and the SV40 polyA.

The following lentivirus gene expression vector was used:

pLV-EF1alpha-murine194-1BBz-P2A-GFP-WPRE-BGH polyA

This construct's gene expression cassette is identical to plasmid (1), only cloned into the vectorbuilder.com lentiviral backbone (third generation).

Cell lines

Both the Eμ-ALL01 cell line (a gift from M. Sadelain; Memorial Sloan-Kettering Cancer Center, New York, New York)[6] and the B16F10 melanoma cell line (American Type Culture Collection) were cultured in complete RPMI 1640 medium with 10% heat-inactivated fetal bovine serum (FBS), 2 mM L-glutamine, 1.5 gl^{-1} sodium bicarbonate, 4.5 gl^{-1} glucose, 10 mM HEPES, 1.0 mM sodium pyruvate and 0.05 mM 2-mercaptoethanol. The immunophenotype and geneexpression pattern have been characterized in ref. [6], and the results demonstrate that Ep-ALL01 cells have a progenitor B-cell phenotype (B220$^+$ CD19$^+$ CD43$^+$ BP1$^+$ HSA$^-$ IgM$^-$). The HEK 293T lentiviral packaging cell line (Clontech) was cultured in DMEM containing 10% FBS, 2 mM glutamate, 100 U ml^{-1} penicillin and 100 μg ml^{-1} streptomycin. For *in vivo* bioluminescent imaging, the Eμ-ALL01 cell line was retrovirally transduced with firefly luciferase (F-luc). All cell lines tested negative for mycoplasma using a DNA-based PCR test (DDC Medical).

MTAS-NLS peptide synthesis

The previously described MTAS-NLS peptide, encompassing a microtubule-associated sequence (MTAS) and a nuclear localization signalling (NLS) sequence[4]: GRYLTQETNKVETYKEQPLKTPGKKKKGKPGKRKEQEKKKRRTR was custom synthesized by AnaSpec Inc. A cysteine was added to the N-terminus of the peptide for linkage to the PBAE-447 polymer.

PBAE 447 synthesis

PBAE 447 was synthesized using a method similar to that in ref. [3]. 1,4-butanediol diacrylate was combined with 4-amino-1-butanol in a 1.1:1 molar ratio of diacrylate monomer to amine monomer. These were heated to 90 °C with stirring for 24 h to produce acrylate-terminated poly(4-amino-1-butanol-co-1,4-butanediol diacrylate). 2.3 g of this polymer was

dissolved in 2 ml tetrahydrofuran (THF). To form the piperazine-capped 447 polymer, 786 mg of 1-(3-aminopropyl)-4-methylpiperazine was dissolved in 13 ml THF then added to the polymer/THF solution. The resulting solution was stirred at room temperature (RT) for 2 h. The capped polymer was precipitated with 5 volumes of diethyl ether. The ether was decanted, then the collected polymer was washed with 2 volumes of fresh ether. The polymer residue was dried under vacuum for 2 days. Neat polymer was dissolved in dimethyl sulfoxide (DMSO) to a concentration of 100 mg ml^{-1} and stored at –20 °C.

PBAE 447–NLS-MTAS peptide conjugation

A solution of 12 mg 4-(maleinimido) phenyl isocyanate (PMPI) in DMSO (20 mg ml^{-1}) was added to 86 mg 447 polymer in DMSO (100 mg ml^{-1}). The solution was mixed at RT for 3 h. The 447-maleimide derivative was added to a solution of 100 mg NLS-MTAS peptide in 5.3 ml DMSO containing tris(2-carboxyethyl)phosphine hydrochloride (TCEP•HCl; 3 mg ml^{-1}). The solution was mixed at RT for 3 h then filtered through a 7k Zeba spin column equilibrated with DMSO. The DMSO was evaporated under vacuum overnight. The 447-peptide conjugate was redissolved in DMSO to 100 mg ml^{-1} 447 and stored at –20 °C.

Cy5-labelling of DNA

Plasmid DNA was labelled with Cy5 using the Mirus Label IT Nucleic Acid Labeling Kit with some modifications to the manufacturer's protocol. The labelling reaction was incubated at 37 °C for 2 h using a 1:4 ratio of labelling reagent to DNA (v:w). The labelled DNA was purified by ethanol precipitation.

PGA–antibody conjugation

Polyglutamic acid (PGA) was dissolved in water to 20 mg ml^{-1} then sonicated for 10 min in a bath sonicator. An equal volume of ethyl-N'-(3-dimethylaminopropyl)carbodiimide•HCl in water (4 mg ml^{-1}, 16 equiv.) was added and the solution was mixed at RT for 5 min. The resulting activated PGA was added to a solution of antibody (*In Vivo*MAb anti-mouse CD3ε F(ab′)2 fragments from Bioxcell.com; cat. no. BE0001-1FAB) in phosphate-buffered saline (PBS) at a 4:1 molar ratio and mixed at RT for 6 h. Excess reagents were removed by dialysis (20,000 MWCO Slide-A-Lyzer Dialysis Cassette) against PBS for 24 h, followed by filtration through a 40k Zeba spin column. Antibody concentration was determined using a NanoDrop 2000 Spectrophotometer (Thermo Scientific).

Nanoparticle preparation

All components were diluted in sodium acetate buffer (25 mM, pH 5.2) to the following concentrations: DNA, 0.1 mg ml^{-1}; PBAEs 447 and 447–NLS-MTAS, 3.14 mg ml^{-1}; PGA-antibody, 0.45 mg ml^{-1} Ab. To prepare the particles, 447–NLS-MTAS was added to DNA at a PBAE:DNA mass ratio of 15:1. The mixture was vortexed gently for 10 s then incubated at RT for 2 min. Unconjugated 447 was then added to the complex at a PBAE:DNA mass ratio of 15:1. The mixture was vortexed gently for 10 s then incubated at RT for 5 min. PGA-antibody was then added at an Ab:DNA mass ratio of 2.5:1. The mixture was vortexed gently for 10 s then incubated at RT for 5 min. Sucrose was added as a cryoprotectant to a final concentration of 30 mg ml^{-1}. The mixture was vortexed briefly, frozen in liquid N$_2$,

then lyophilized using a FreeZone 2.51 Freeze Dry System (Labconco). Lyophilized particles were resuspended in water at 1/3 of the pre-lyophilization volume.

Nanoparticle characterization

The number, average hydrodynamic radius and concentration of the nanoparticles were determined using a NanoSight NS300 instrument (Malvern Instruments). Lyophilized particles were resuspended in water at the same concentration used for transfection. After gentle vortexing, the particles were incubated on ice for 10 min to allow for complete hydration. The suspension was centrifuged for 3 min at $2,400g$, then the supernatant was diluted 5-fold for Nanoparticle Tracking Analysis. The zeta potential of the particles was determined using a ZetaPALS Zeta Potential Analyzer (Brookhaven Instruments Corporation). Freshly prepared nanoparticles were centrifuged for 1 min at $1,000g$, then the supernatant was diluted 14× in PBS for these measurements.

Transmission electron microscopy

25 µl of freshly made nanoparticles was deposited on a glow discharge-treated 200 mesh carbon/Formvar-coated copper grid. After 30 s, the grid was touched sequentially to a drop of ½ Karnovsky's fixative, a drop of 0.1 M cacodylate buffer, 8 drops of dH_2O (distilled water), then a drop of 1% (w/v) filtered uranyl acetate. The grid was run over filter paper with a strip of dH_2O, then dried overnight in a desiccator. Samples were imaged with a JEOL JEM-1400 transmission electron microscope operating at 120 kV (JEOL USA).

In vitro T-cell transfection using synthetic DNA nanocarriers

Spleens of C57BL/6J mice were macerated over a filter, and resuspended in ACK lysing buffer (Biosource). Effector $CD8^+$ T cells were prepared by incubating splenocytes (3×10^6 ml^{-1}) in complete RPMI 1640 with 1 ng ml^{-1} interleukin-7 (PeproTech) and 2 µg ml^{-1} Concavalin A (Calbiochem) at 37°C. Two days later, dead cells were removed by Ficoll gradient separation (GE Healthcare) and $CD8^+$ cells were isolated using a mouse CD8 Negative Isolation Kit (Stemcell Technologies). Cells were captured by passing them over a syringe filter with a 1-µm pore size. Subsequently, the filter was loaded (Fig. 2c) with the nanoparticle suspension, using the particle concentrations indicated in the figures, and allowed to empty by gravity flow. To release nanoparticle-transfected T cells, we reversed the filter and flushed it three times with complete RPMI 1640 supplemented with 10 ng ml^{-1} interleukin-2.

Functional in vitro T-cell assays

Cytotoxicity assay—We measured *in vitro* cytotoxic activity of T cells using standard flow cytometry-based assays as described elsewhere[31]. Briefly, Eµ-ALL01 leukaemia cells (or B16F10 melanoma tumour cells as controls) were labelled with the membrane dye PKH-26 (Sigma-Aldrich), washed with RPMI containing 10% foetal calf serum, and resuspended in the same medium at a concentration of 1×10^5 tumour cells per ml. T cells were added to the suspensions at varying effector-to-target cell ratios in 96-well plates (final volume, 200 µl) and incubated for 3h at 37 °C. Then, cells were transferred to V-bottom 96-

well plates and stained with Annexin V-Brilliant Violet 421 (BioLegend). Following a wash in PBS, the cells were analysed by flow cytometry.

Cytokine secretion assay—T-cell cytokine release was measured with ELISA (R&D Systems) 24 h (IL-2) or 48 h (IFN-γ and TNF-α) after stimulation on irradiated Eμ-ALL01 leukaemia cells or B16F10 melanoma controls.

Southern blot analysis

DNA of T cells (either nanoparticle-transfected and GFP-sorted, or untransfected) was digested with the restriction enzymes *Not*I and *Xma*I (New England Biolabs) that cleave within the transposon sequence to produce an internal 750-bp fragment. Following digestion, approximately 10 μg DNA was electrophoresed, transferred to a Hybond-N+ membrane (GE Healthcare), and hybridized using QuickHyb hybridization solution (Stratagene) following the manufacturer's recommendations. For hybridization, a 500-bp probe specific for the 750-bp fragment was generated by PCR amplification from 10 pg transposon-containing plasmid DNA and labelled with a Rediprime II DNA Labeling System (GE Healthcare) following the manufacturer's recommendations.

Mice and *in vivo* tumour models

Mice were housed in the animal facility at Fred Hutchinson Cancer Research Center, and used in the context of a protocol approved by the Center's Institutional Animal Care and Use Committee. We modelled haematological cancers by systemically injecting luciferase-expressing Eμ-ALL01 leukaemia cells[6] into 4–6-week-old female albino B6 (C57BL/6J-Tyr < c-2J>) mice (Jackson Laboratories) and allowing them to develop for 1 week. Following tail-vein injection of Eμ-ALL01 leukaemia cells, all animals were included in our studies and included in the analysis, and the mice were randomly assigned to experimental cohorts. They were then treated daily for 5 days with 3×10^{11} CD3-targeted nanoparticles carrying CAR-transgenes (or control particles) in a suspension that was administered slowly over 20 min through a rodent tail-vein catheter using a programmable BS-300 infusion pump (both Braintree Scientific Inc.). To compare the therapeutic efficacy of nanoparticle infusions with conventional adoptive T-cell therapy, one group of mice was treated with a single dose of 5 million T cells transduced *ex vivo* with a murine194-1BBz CAR-encoding lentiviral vector. Only these mice were preconditioned with 100 mg kg^{-1} cyclophosphamide intraperitoneally to eliminate endogenous lymphocytes a day before T-cell transfer.

Lentiviral production and *ex vivo* T-cell transduction

Lentiviral stocks were generated by transfection of 293T cells with the *pLV-EF1alpha-murine194-1BBz-P2A-GFP-WPRE-BGH polyA* plasmid described above (pCMVdeltaR8.91) and pMD.G (both plasmids were purchased from Addgene) followed by concentration as previously reported[32]. For lentiviral gene transfer into murine T cells, 1 ml per well of lentivirus was preloaded on 6-well non-tissue-culture-treated dishes coated with RetroNectin (TakaraBio) and incubated at 37 °C for 1 h. An equal volume of Concavalin A/IL-7 activated T lymphocytes (3×10^6 cells per ml^{-1} in RPMI medium supplemented with 50 IU hIL-2 ml^{-1}) was added and centrifuged at 2,000g for 30 min. Six hours after

spinoculation, 1 ml of fresh, prewarmed RPMI containing 50 IU hIL-2 (Chiron) was added. T cells were used for adoptive transfer experiments 2 days after gene transfer.

In vivo bioluminescence and fluorescence imaging

We used D-luciferin (Xenogen) in PBS (15 mg ml^{-1}) as a substrate for F-luc (used for imaging of Eμ-ALL01 leukaemia cells) and CBR-luc[30] (used for T-cell imaging). Bioluminescence images were collected with a Xenogen IVIS Spectrum Imaging System (Xenogen). Living Image software version 4.3.1 (Xenogen) was used to acquire (and later quantitate) the data 10 min after intraperitoneal injection of D-luciferin into animals anesthetized with 150 mg kg^{-1} of 2% isoflurane (Forane, Baxter Healthcare). Acquisition times ranged from 10 s to 5 min. To correct for background bioluminescence, we subtracted signals acquired from tumour-free mice (injected with D-luciferin) from the measurement region of interest (ROI).

For *in vivo* fluorescence biodistribution studies (Fig. 4), we loaded CD3-targeted or non-targeted polymer nanoparticles with Cy5-labelled plasmid DNA. To extract the signal emitted by the Cy5 fluorophore (excitation (ex): 647 nm, emission (em): 665 nm) from tissue autofluorescence, an image sequence (ex: 465 nm, em, 520 nm/ex: 535 nm, em: 600 nm/ex: 570 nm, em: 620 nm/ex: 675 nm, em: 720 nm; f/stop 2, which is a measure of the lens aperture, 10 s) was collected with the imaging system, and spectrally unmixed using Living Image software. Before all bioimaging experiments, Nair depilatory cream (Church and Dwight) was applied to the C57Bl/6 mice and washed off to remove hair.

Nanoparticle biodistribution

C57Bl/6 mice were intravenously injected with 3×10^{11} Cy5-tagged nanoparticles that were either non-targeted, or targeted to the T-cell CD3 molecule. The nanoparticle suspension was administered through a tail vein as described above. After 6 h, tissues as indicated were removed, weighed and macerated as needed with scissors. We quantified specific Cy5 tissue fluorescence for each organ using the IVIS Spectrum imaging system, and calculated the percentage of injected dose per gram of tissue (%ID g^{-1}) as the final readout.

Toxicity studies

To measure potential *in vivo* toxicities of repeatedly infusing lymphocyte-targeted DNA nanocariers, we injected mice intravenously with five sequential doses of 3×10^{11} CD3-targeted nanoparticles carrying P4-1BBz CAR-encoding transgenes over the course of 5 days. Control animals received no treatment. Each experimental group comprised 10 mice. Twenty-four hours after the final nanoparticle infusion, mice were anesthetized and blood was collected by retro-orbital bleed using heparinized microcapillary tubes into ethylenediaminetetraacetic acid-containing microcontainers for determination of the complete blood count (CBC), which included a white blood cell count with differential, a red blood cell count, haemoglobin, haematocrit, and a platelet count. Blood was also collected into serum separator tubes for serum chemistry and cytokine profile analyses (performed by AniLytics Inc.). Animals were then euthanized with carbon dioxide to retrieve organs, which were washed with deionized water before fixation in 4% paraformaldehyde. The tissues were processed routinely, and sections were stained with

hematoxylin and eosin. The specimens were interpreted by S. Pillai, a board-certified staff pathologist, in a blinded fashion.

Flow cytometry and cell sorting

All flow cytometry antibodies were purchased from ebioscience. Cells were acquired on a FACSCanto Flow Cytometer (BD Biosciences). For experiments involving fluorescence-activated cell sorting (Figs 2e–h and 3a), a FACSAria III cell sorter (BD Biosciences) was used.

Confocal microscopy

Cells were transferred onto fibronectin (Sigma Aldrich)-coated 10-mm teflon ring glass slides (Esco), fixed in 2% paraformaldehyde, mounted with ProLong Gold Antifade reagent (Invitrogen) for 24 h, and imaged with a Zeiss LSM 780 confocal microscope.

Statistical methods

Pairwise differences in bioluminescent tumour and T-cell signals were analysed at selected time points using the Wilcoxon rank-sum test, and we characterized survival data using the Log-rank test. We treated 10 animals per group, which provided 80% power to detect an effect size of 1 standard deviation between groups, based on a t-test with a two-sided significance level of 0.05. With the exception of the toxicity studies, investigators conducting the experiments were not blinded. All statistical analyses were performed using GraphPad Prism software version 6.0.

Supplementary Material

Refer to Web version on PubMed Central for supplementary material.

Acknowledgments

References

1. Rosenberg SA, Restifo NP. Adoptive cell transfer as personalized immunotherapy for human cancer. Science. 2015; 348:62–68. [PubMed: 25838374]

2. Plumridge, H. New costly cancer treatments face hurdles getting to patients. The Wall Street Journal. Oct 6. 2014 https://www.wsj.com/articles/new-costly-cancer-treatments-face-hurdles-getting-to-patients-1412627150

3. Mangraviti A, et al. Polymeric nanoparticles for nonviral gene therapy extend brain tumor survival in vivo. ACS Nano. 2015; 9:1236–1249. [PubMed: 25643235]

4. Narayanan K, et al. Mimicking cellular transport mechanism in stem cells through endosomal escape of new peptide-coated quantum dots. Sci Rep. 2013; 3:2184. [PubMed: 23851637]

5. Maude SL, et al. Chimeric antigen receptor T cells for sustained remissions in leukemia. N Engl J Med. 2014; 371:1507–1517. [PubMed: 25317870]

6. Davila ML, Kloss CC, Gunset G, Sadelain M. CD19 CAR-targeted T cells induce long-term remission and B cell aplasia in an immunocompetent mouse model of B cell acute lymphoblastic leukemia. PLoS ONE. 2013; 8:e61338. [PubMed: 23585892]

7. Nakazawa Y, et al. Evaluation of long-term transgene expression in piggyBac-modified human T lymphocytes. J Immunother. 2013; 36:3–10. [PubMed: 23211626]

8. Burnight ER, et al. A hyperactive transposase promotes persistent gene transfer of a piggyBac DNA transposon. Mol Ther Nucleic Acids. 2012; 1:e50. [PubMed: 23344650]

9. Gade TP, et al. Targeted elimination of prostate cancer by genetically directed human T lymphocytes. Cancer Res. 2005; 65:9080–9088. [PubMed: 16204083]

10. Maude SL, Teachey DT, Porter D, Grupp SA. CD19-targeted chimeric antigen receptor T-cell therapy for acute lymphoblastic leukemia. Blood. 2015; 125:4017–4023. [PubMed: 25999455]

11. Grupp SA, et al. Chimeric antigen receptor-modified T cells for acute lymphoid leukemia. N Engl J Med. 2013; 368:1509–1518. [PubMed: 23527958]

12. Rosenberg SA. Cell transfer immunotherapy for metastatic solid cancer—what clinicians need to know. Nat Rev Clin Oncol. 2011; 8:577–585. [PubMed: 21808266]

13. Wang X, et al. Large-scale clinical-grade retroviral vector production in a fixed-bed bioreactor. J Immunother. 2015; 38:127–135. [PubMed: 25751502]

14. Kuchenbaecker KB, et al. Identification of six new susceptibility loci for invasive epithelial ovarian cancer. Nat Genet. 2015; 47:164–171. [PubMed: 25581431]

15. Johnson LA, et al. Rational development and characterization of humanized anti-EGFR variant III chimeric antigen receptor T cells for glioblastoma. Sci Transl Med. 2015; 7:275ra222.

16. Magnani CF, et al. Immunotherapy of acute leukemia by chimeric antigen receptor-modified lymphocytes using an improved sleeping beauty transposon platform. Oncotarget. 2016; 7:51581–51597. [PubMed: 27323395]

17. Abate-Daga D, et al. A novel chimeric antigen receptor against prostate stem cell antigen mediates tumor destruction in a humanized mouse model of pancreatic cancer. Hum Gene Ther. 2014; 25:1003–1012. [PubMed: 24694017]

18. Sadelain M. CAR therapy: the CD19 paradigm. J Clin Invest. 2015; 125:3392–3400. [PubMed: 26325036]

19. Meacham CE, Morrison SJ. Tumour heterogeneity and cancer cell plasticity. Nature. 2013; 501:328–337. [PubMed: 24048065]

20. Li X, et al. Nanoparticle-mediated transcriptional modification enhances neuronal differentiation of human neural stem cells following transplantation in rat brain. Biomaterials. 2016; 84:157–166. [PubMed: 26828681]

21. Kim J, Kang Y, Tzeng SY, Green JJ. Synthesis and application of poly (ethylene glycol)-co-poly(beta-amino ester) copolymers for small cell lung cancer gene therapy. Acta Biomater. 2016; 41:293–301. [PubMed: 27262740]

22. Zhang X, Edwards JP, Mosser DM. The expression of exogenous genes in macrophages: obstacles and opportunities. Methods Mol Biol. 2009; 531:123–143. [PubMed: 19347315]

23. Marodon G, et al. Specific transgene expression in human and mouse CD4+ cells using lentiviral vectors with regulatory sequences from the CD4 gene. Blood. 2003; 101:3416–3423. [PubMed: 12511423]

24. Ellmeier W, Sunshine MJ, Losos K, Hatam F, Littman DR. An enhancer that directs lineage-specific expression of CD8 in positively selected thymocytes and mature T cells. Immunity. 1997; 7:537–547. [PubMed: 9354474]

25. Wu CY, Rupp LJ, Roybal KT, Lim WA. Synthetic biology approaches to engineer T cells. Curr Opin Immunol. 2015; 35:123–130. [PubMed: 26218616]

26. Kebriaei P, et al. Phase I trials using sleeping beauty to generate CD19-specific CAR T cells. J Clin Invest. 2016; 126:3363–3376. [PubMed: 27482888]

27. Monjezi R, et al. Enhanced CAR T-cell engineering using non-viral sleeping beauty transposition from minicircle vectors. Leukemia. 2017; 31:186–194. [PubMed: 27491640]

28. Brooks PJ, Yang NN, Austin CP. Gene therapy: the view from NCATS. Hum Gene Ther. 2016; 27:7–13. [PubMed: 26784641]

29. Gaspar V, et al. Minicircle DNA vectors for gene therapy: advances and applications. Expert Opin Biol Ther. 2015; 15:353–379. [PubMed: 25539147]

30. Dobrenkov K, et al. Monitoring the efficacy of adoptively transferred prostate cancer-targeted human T lymphocytes with PET and bioluminescence imaging. J Nucl Med. 2008; 49:1162–1170. [PubMed: 18552144]

31. Fischer K, Andreesen R, Mackensen A. An improved flow cytometric assay for the determination of cytotoxic T lymphocyte activity. J immunol Methods. 2002; 259:159–169. [PubMed: 11730851]

32. May C, et al. Therapeutic haemoglobin synthesis in β-thalassaemic mice expressing lentivirus-encoded human β-globin. Nature. 2000; 406:82–86. [PubMed: 10894546]
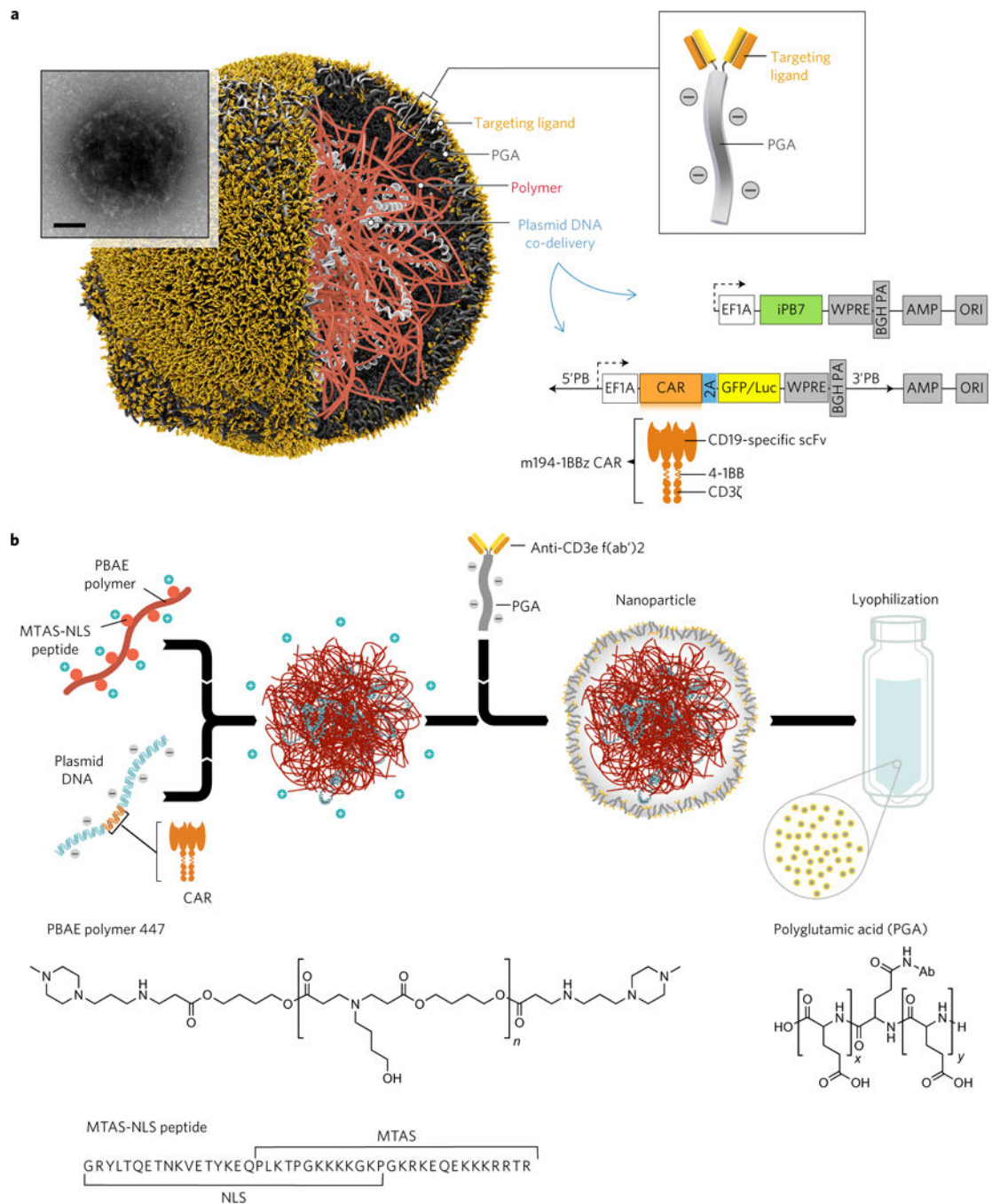
Figure 1. Design and manufacture of lymphocyte-programming nanoparticles

a, Schematic of the T-cell-targeted DNA nanocarrier used in our experiments. The inset shows a transmission electron micrograph of a representative nanoparticle. Scale bar, 100 nm. Also depicted are the two plasmids that were encapsulated into the nanoparticles; these encode an all-murine 194-1BBz CAR and the hyperactive iPB7 transposase. EF1A, eukaryotic translation elongation factor 1 alpha 1; BGH PA, bovine growth hormone polyadenylation signal; ampicillin resistance gene; ORI, origin of replication. **b**, Diagram describing the fabrication of the poly(β-amino ester) nanoparticles. Also shown are the

chemical structures of the PBAE 447 polymer and polyglutamic acid, as well as the amino acid sequence of the microtubule-associated-nuclear localization (MTAS-NLS) peptide.
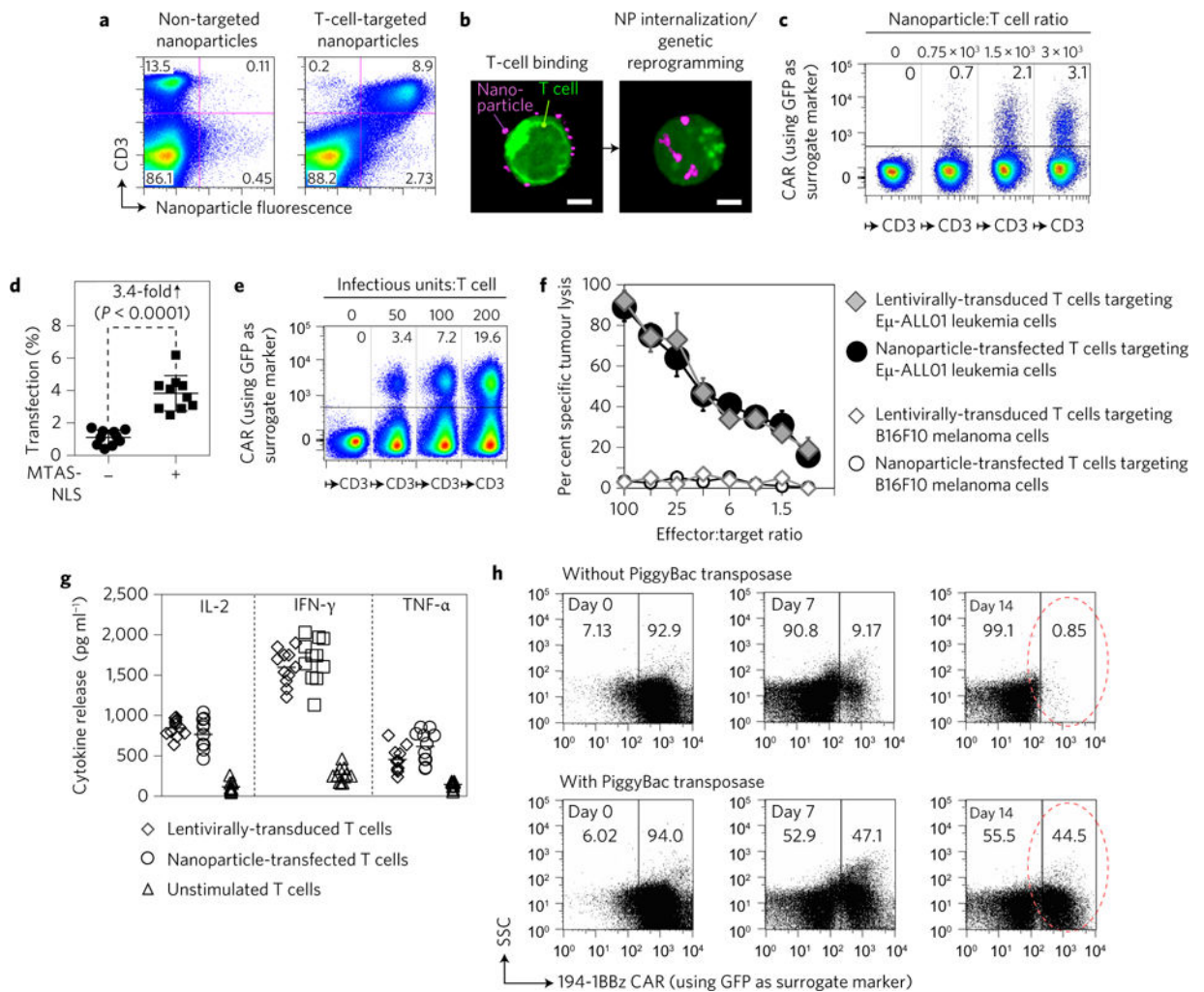
Figure 2. DNA nanocarriers choreograph robust and persistent CAR production by lymphocytes *in vitro*

a, Flow cytometry of nanoparticles binding to T cells. Splenocytes from naive C57BL/6 mice were mixed with CD3-targeted nanoparticles carrying Cy5-labelled plasmid DNA. After a 20-min incubation, cells were washed to remove unbound particles, and analysed by flow cytometry. The profiles shown here are representative of eight independent experiments. **b**, Confocal microscopy establishes that nanoparticles loaded with Cy5-labelled DNA (magenta) are rapidly (within 120 min) internalized from the cell surface. To provide contrast, T cells were labelled with CellTracker Green prior to nanoparticle exposure. The images are representative of 20 randomly chosen fields. Scale bars, 2 μm. **c**, Flow cytometry of T cells 30 h after incubation with nanoparticles bearing 194-1BBz_2A_GFP genes. The graph displays CD3$^+$-gated lymphocyte populations. **d**, Comparison of T-cell transfection efficiencies achieved with DNA nanocarriers that contain microtubule-associated and nuclear localization signalling peptide sequences with those that do not, based on 10 independent experiments. **e**, Flow cytometry of T cells 30 h after transduction with a lentiviral vector encoding the same 194-1BBz_2A_GFP construct. The numbers within the graphs in **c** and **e** show the percentage of CAR + T cells (using GFP as

surrogate marker). **f**, *In vitro* assay comparing cytotoxicity of nanoparticle-transfected versus lentivirus-transfected T cells against Eµ-ALL01 leukaemia cells, or the B16F10 cell line as a control. To ensure equal CAR expression levels, transfected T cells were sorted using FACS to GFP mean fluorescence intensities (as a surrogate reporter for CAR expression) between 10^3 and 10^4 before using them in the functional assays. Each point represents the mean ± s.e.m. pooled from independent experiments conducted in triplicate. **g**, ELISA measurements of IL-2 (at 24 h), and IFN-γ and TNF-α (at 48 h) secretion by transfected cells following co-culture with Eµ-ALL01 leukaemia cells. Unstimulated, lentivirus-transduced 194-1BBz CAR T-cells were analysed for comparison. **h**, Co-delivery of plasmids encoding the hyperactive piggyBac transposase iPB7 promotes persistent CAR gene expression. After transfection and sorting, CAR-positive T cells were cultured and the persistence of their 194-1BBz_2A_GFP expression was measured with flow cytometry. Data are representative of two independent experiments.
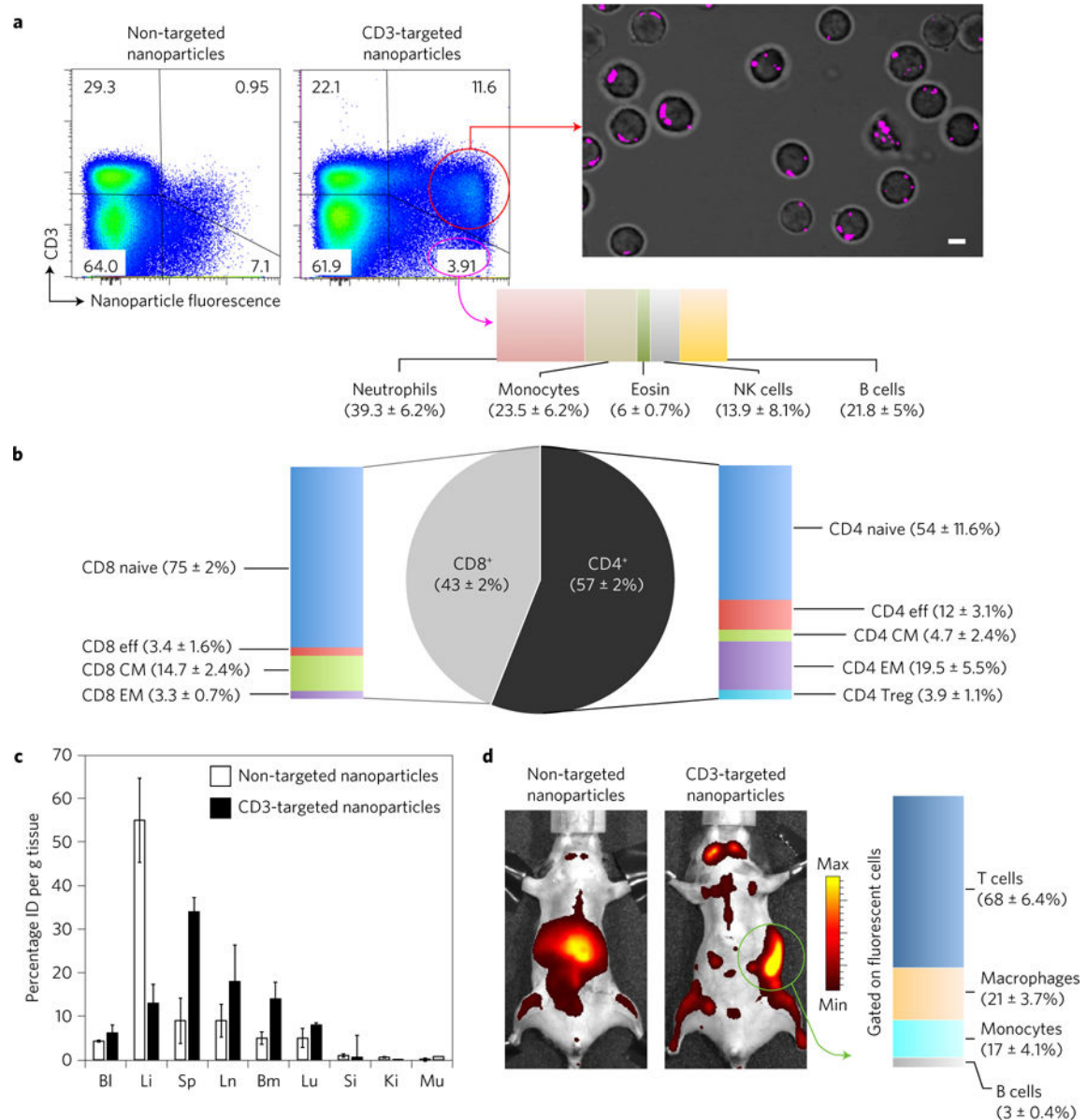
Figure 3. CD3-targeted nanoparticles bind to circulating T cells in mice

a, Flow cytometry demonstrating fluorescent nanoparticle binding to peripheral T cells 4 h after a 3×10^{11} dose was injected. The right panel is confocal microscopy of CD3-sorted T cells, establishing that, like *in vitro*, the particles are rapidly internalized from the surfaces of circulating cells. Shown below are the phenotypes of other circulating cell subtypes that non-specifically bound the injected nanoparticles, as measured by flow cytometry: neutrophils (Ly6G$^+$, CD11b$^+$, CD11c$^-$), monocytes (Ly6C$^+$, CD11b$^+$, CD11c$^-$), eosinophils (CD11b$^+$, CD193$^+$, F4/80$^+$), natural killer (NK) cells (CD49b$^+$, NKp46$^+$), B cells (B220$^+$). Data are representative of two independent experiments with two animals per treatment group. Scale bar, 3 μm. **b**, Phenotypes of circulating T cell subtypes internalizing injected nanoparticles, as measured by flow cytometry: naive T cells (CD62L$^+$, CD44$^-$), effector T cells (CD62L$^-$, CD44$^+$), central memory (CM) T cells (CD62L^{high}, CD44$^+$), effector

memory (EM) T cells (CD62L^{low}, CD44$^+$), and regulatory T (Treg) cells (CD4$^+$, Foxp3$^+$, CD25$^+$). The CD4:CD8 ratio of nanoparticle-transfected T cells is shown as a pie chart in the centre; the bar graphs on the sides reflect percentages of each T-cell subtype. **c**, Biodistribution of fluorescent T-cell-targeted or non-targeted nanoparticles 4 h after tail-vein injection. Data are expressed as injected dose (ID) per gram of tissue. Bl, blood; Li, liver; Sp, spleen; Ln, lymph node; Bm, bone marrow; Lu, lung; Si, small intestine; Ki, kidney; Mu, muscle. Data are from ten mice per treatment condition pooled from two independent experiments. Each bar represents the mean percentage of ID per gram tissue ± s.e.m. **d**, Bioimaging of nanoparticle distributions. One representative mouse from each cohort ($n =$ 10) is shown. A bar graph on the right reflects percentages of splenocytes positive for fluorescent nanoparticles in animals treated with CD3-targeted nanoparticles, as measured by flow cytometry: T cells (CD3$^+$), macrophages (F4/80$^+$, CD11b$^+$, CD11c$^−$), monocytes (CD11b$^+$, Gr1$^+$, F4/80^{low}), and B cells (B220$^+$).
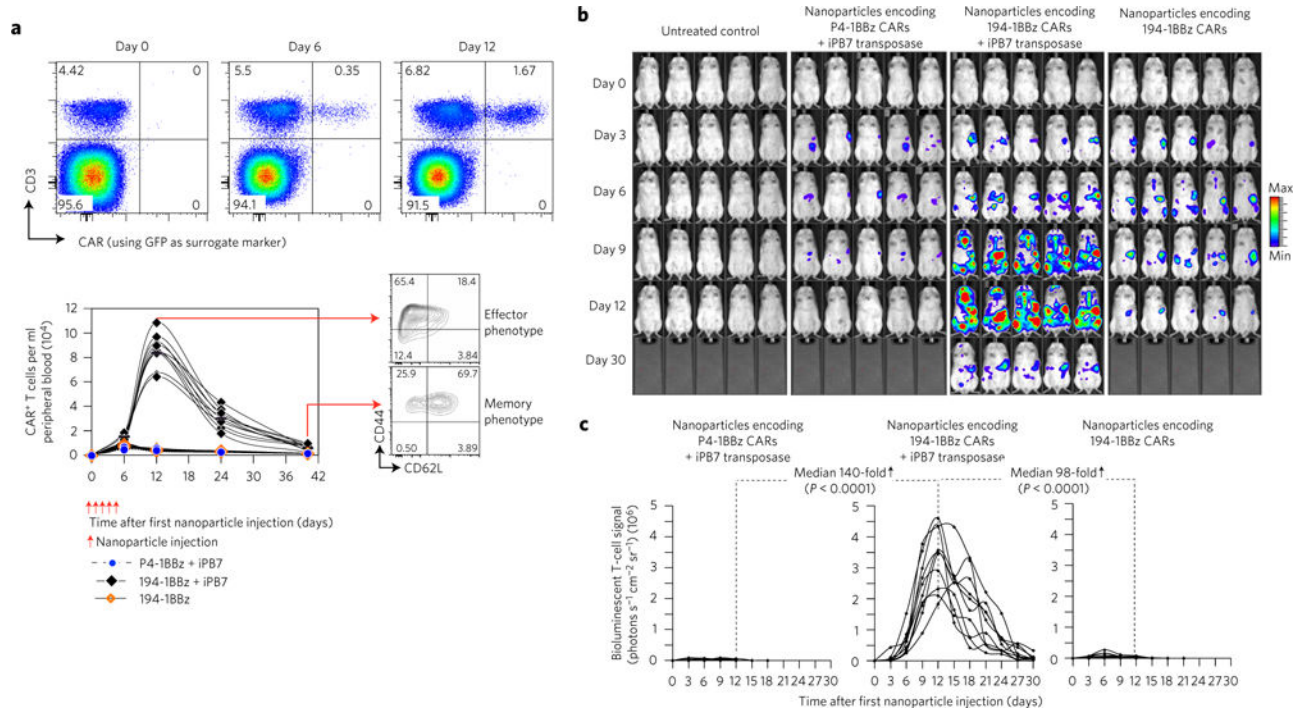
Figure 4. Reprogramming host T cells with leukaemia-specific CAR genes
a, Top: flow cytometry of peripheral T cells following injection of nanoparticles delivering DNA that encodes 194-1BBz_2A_GFP or tumour-irrelevant P4-1BBz_2A_GFP genes. The profiles shown here are representative of two independent experiments consisting of five mice per group. Bottom: to determine whether persistent CAR expression in actively dividing T cells requires co-delivery of plasmid encoding the hyperactive transposase, we also compared 194-1BBz transgene-loaded nanocarriers containing or lacking iPBS7 transgenes. **b**, Sequential bioimaging of nanoparticle-programmed CAR+ T cells. In this experiment, nanoparticles were loaded with plasmids that co-express the click beetle red luciferase (CBR-luc) reporter along with the CAR transgene. As in the previous experiments (panel **a**), 194-1BBz CAR-encoding nanoparticles were prepared with or without iPB7 transgenes. Five representative mice from each cohort ($n = 10$) are shown. **c**, Plots of CBR-luc signal intensities after nanoparticle injections. Each line represents one animal and each dot reflects its whole animal photon count. Pairwise differences in photon counts between treatment groups were analysed using the Wilcoxon rank-sum test. Shown are data for ten mice per treatment condition pooled from three independent experiments.
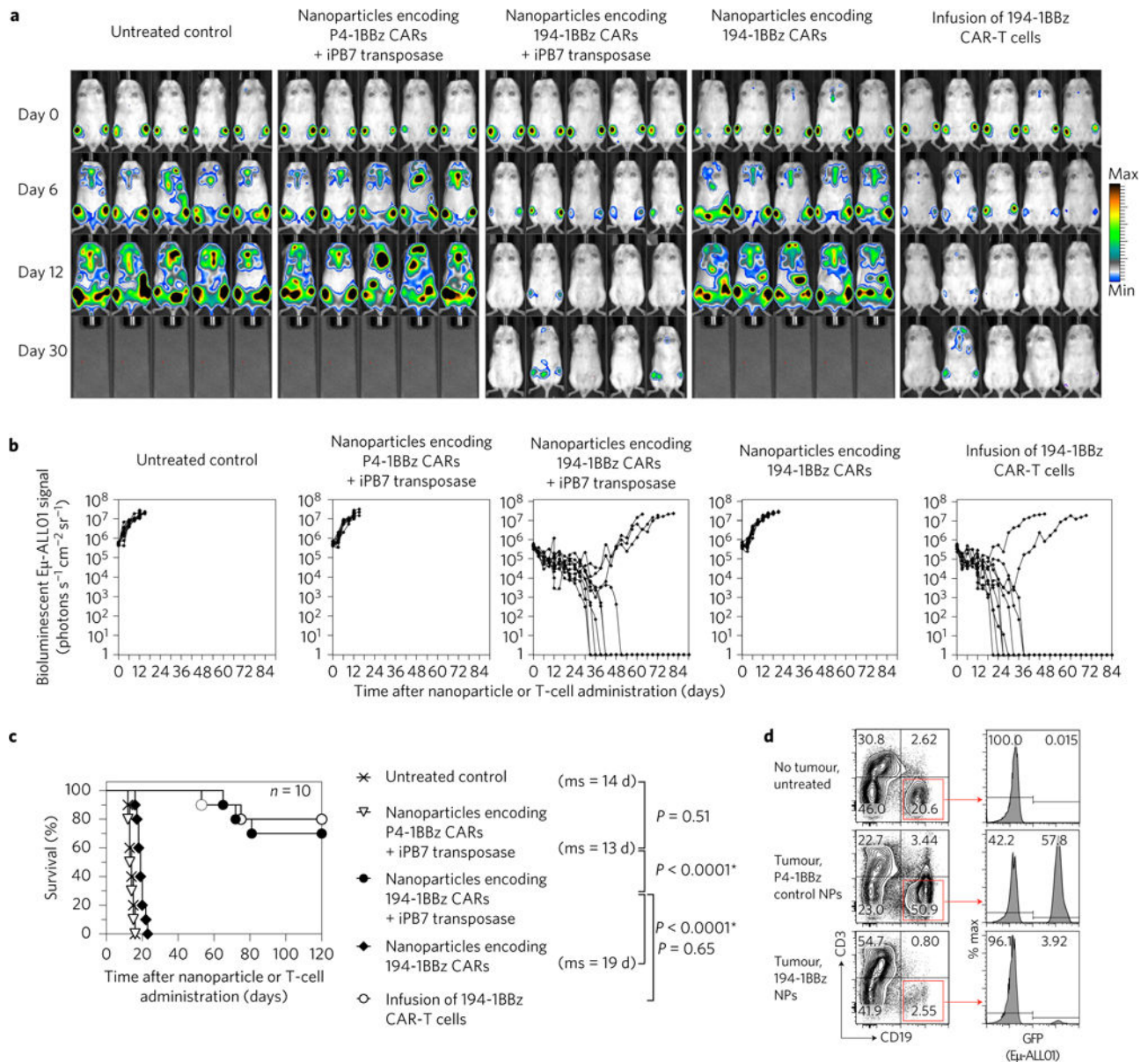
Figure 5. Nanoparticle-programmed CAR lymphocytes can cause tumour regression with efficacies similar to adoptive T-cell therapy

a, Sequential bioimaging of firefly luciferase-expressing Eμ-ALL01 leukaemia cells systemically injected into albino C57BL/6 mice. One week after this injection (Day 0), the animals were treated with five sequential injections (Day 0-Day 5) of 3×10^{11} lymphocyte-targeting nanoparticles carrying 194-1BBz or P4-1BBz CAR-encoding transgenes. To test whether integration of nanoparticle-delivered CAR transgenes into the chromosomes of *in situ* reprogrammed T cells is a requirement to achieve anti-leukaemia effects, we injected 194-1BBz transgene-loaded nanocarriers with or without iPBS7 transgenes into two different treatment groups. Controls were not treated. An additional group of mice was first given cyclophosphamide, then a day later treated with a single dose of 5 million CAR^{+} T cells that had been transduced ex *vivo* with 194-1BBz-encoding lentiviral vectors. Five

representative mice from each cohort ($n = 10$) are shown. **b**, Quantification of the results shown in **a**. Every line represents one animal and each dot reflects the whole animal photon count. **c**, Survival of animals following therapy, depicted as Kaplan-Meier curves. Shown are ten mice per treatment group pooled from three independent experiments. ms, median survival. Statistical analysis between the treated experimental and the untreated control group was performed using the Log-rank test; $P < 0.05$ was considered significant. **d**, Flow cytometry plots showing killing of malignant and normal B cells 12 days after treatment with 194-1BBz-encoding nanoparticles. The numbers labelling the peaks represent percentage of GFP-negative (left) and GFP-positive (right) cells. The leukemia cells were GFP-positive, whereas the endogenous B cells are GFP-negative. To distinguish leukaemia from healthy B lymphocytes, Eµ-ALL01 cells were genetically tagged with GFP. The respective subsets are illustrated in separate histogram plots that are gated on CD19^{+} cell populations. Data are representative of ten mice per treatment group pooled from three independent experiments.